CRYSTAL GROWTH & DESIGN

pubs.acs.org/crystal

Article

Substrate Chemistry and Lattice Effects in Vapor Transport Growth of Vanadium Dioxide Microcrystals

Samuel T. White,* Ellis A. Thompson, Peyton F. Brown, and Richard F. Haglund*

Cite This: *Cryst. Growth Des.* 2021, 21, 3770−3778

Read Online

ACCESS | Metrics & More | Article Recommendations | Supporting Information

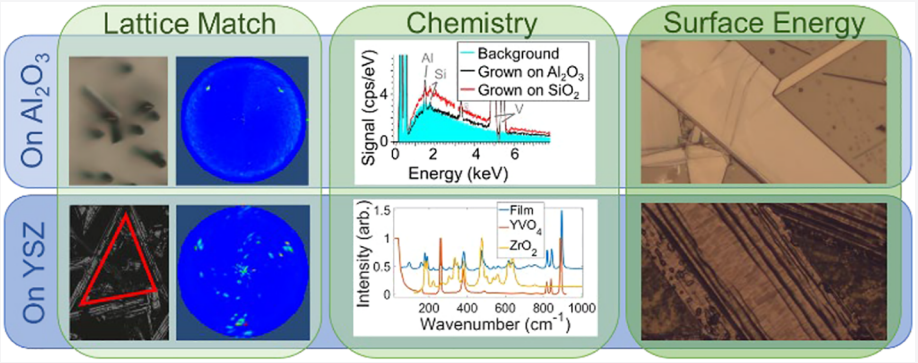

ABSTRACT: Vapor-phase transport is a rapid, inexpensive method of growing nano- and microscale single crystals of vanadium dioxide, a correlated-electron material with a metal−insulator transition at ∼70 °C. Many growth parameters—including time, temperature, precursor, ambient conditions, and substrate—have been explored, and a variety of crystal morphologies has been produced, with most emphasis given to oriented nanowires. However, a comprehensive strategy for predicting/controlling the crystal morphology is still evolving. Here, we investigate the role of the substrate in platelet growth, highlighting three important types of interactions: chemical reactions at the surface, lattice matching effects, and surface energy. We present results on four different cuts of sapphire (Al_2O_3) and three of yttria-stabilized zirconia (YSZ) to differentiate the roles of these mechanisms. Each has significant effects: chemical reactions leading to Al-doped VO_2 on Al_2O_3 and the formation of YVO_4 on YSZ, lattice match producing preferred orientations on both, and high surface energy promoting growth of larger microcrystals. We suggest a framework for relating crystal morphology, orientation, and doping to substrate properties, in order to use intentional choice of the substrate to engineer the size, shape, orientation, and strain state of VO_2 single crystals, a crucial step toward realizing VO_2 crystal-based devices.

INTRODUCTION

Vanadium dioxide (VO_2) remains among the most promising reconfigurable materials[1−6] with tunable optical and electrical properties. Its first-order phase transition from an insulating monoclinic phase (M1) to a metallic rutile phase (R) is accompanied by a change in resistivity by multiple orders of magnitude, sharp change in optical constants, and ∼1% change in lattice strain (shrinking along the c_R axis, expanding normal to it, see Supporting Information, Section S1, Figure S1, and Table S1). This phase transition occurs at the readily accessible temperature of ∼70 °C and can be initiated optically on a femtosecond time scale;[7] moreover, its critical temperature (T_c) and hysteretic response can be tuned via local strain, particle size, and doping,[8] increasing its versatility. VO_2 has been employed in sundry devices, from passive thermal control coatings[9] to ultrafast photonic modulators[10] and the complex physics underlying the phase transition—the role of the structural versus the electronic transition and the difference between thermal and optical excitation—have made it an ideal subject in the study of correlated-electron materials.[2]

Bulk VO_2 single crystals—while less robust and less viable for large-scale applications than thin films—offer high crystalline quality, smooth faceted faces, and, in the absence of substrate strain, sharp, single-domain switching. When subject to strain, VO_2 single crystals exhibit ferroelasticity, with strain-sensitive twin domains that form additional nucleation sites for the phase transition[11] and generate complex patterns of coexisting of metallic and insulating domains.[12] A broad range of applications requiring single-crystal VO_2 have been proposed or demonstrated. Nanowires have been used for nanoactuators, tiny optically readable thermometers, nanoscale gas sensors, thermal rectifiers, and more.[4] Microplatelets have

Received: January 25, 2021
Revised: May 18, 2021
Published: June 2, 2021

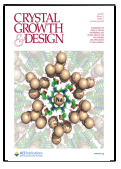

https://doi.org/10.1021/acs.cgd.1c00088
Cryst. Growth Des. 2021, 21, 3770−3778

Table 1. Substrates Used in This Work

substrate	formula	orientation	wafer size
quartz	SiO_2	*z*-cut (0001)	100 mm diameter × 0.5 mm
sapphire	Al_2O_3	*c*-cut (0001)	100 mm diameter × 0.65 mm
		r-cut $(1\bar{1}02)$	2″ diam. × 0.5 mm
		a-cut $(11\bar{2}0)$	10 × 10 × 0.5 mm
		m-cut $(10\bar{1}0)$	10 × 10 × 0.5 mm
YSZ	ZrO_2/Y_2O_3 (92:8)	(100)	10 × 10 × 0.5 mm
		(111)	10 × 10 × 0.5 mm
		(110)	10 × 10 × 0.5 mm

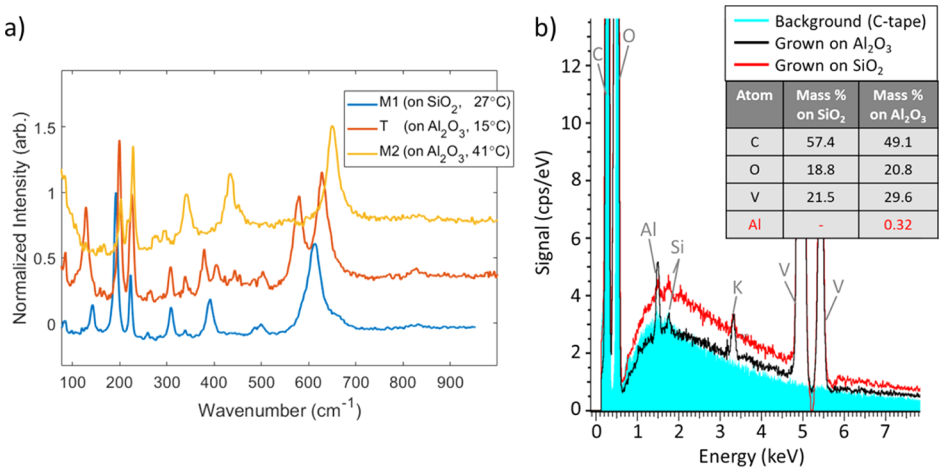

Figure 1. VO_2 crystals grown on sapphire are in the M2 phase at room temperature due to Al-doping. (a) Raman spectra comparing a VO_2 crystal grown on sapphire, above (yellow) and below (red) the M2-T phase transition, to an M1-phase VO_2 crystal grown on quartz. (b) EDS spectrum showing Al-doping of the crystal grown on sapphire.

received less attention but proved to be an ideal platform to demonstrate reconfigurable index-based control of hyperbolic phonon polaritons in hexagonal boron nitride.[13]

The sensitivity of the VO_2 phase transition to so many factors—size and shape, strain state, dopants, and crystal defects—and the variety of potential applications, each with its own specific requirements, necessitate the development of growth techniques that can engineer VO_2 crystals to have desired properties. In the last two decades, vapor transport methods have gained popularity as a way to produce high-quality nano- and microscale crystals at low cost and in a short time.[11,14−28] Numerous growth parameters—including time, temperature, precursors, ambient conditions, and substrate—constitute a set of potential tools for tailoring the resulting crystals. The choice of growth substrate, in particular, has been shown to affect crystal size, shape, and orientation (see Supporting Information, Section S2 and Table S2 for a detailed review of the growth substrates investigated heretofore and their effects). These effects can broadly be separated into two groups: those arising due to lattice match and those arising from chemical reactions between the substrate and VO_2 precursor materials. The former has received by far the most attention and has been exploited to produce highly oriented nanowires of several varieties, while the latter, although not unknown,[26,29] is often overlooked.

In this paper, we explore the possibilities for substrate-driven engineering of vapor transport-grown VO_2 single crystals, highlighting the importance of surface energy and chemical reactions at the V_2O_5/substrate interface, in addition to the lattice matching effects which have already begun to be exploited. We show that Al-doping occurs in VO_2 crystals grown on the commonly used substrate Al_2O_3 and go on to identify the lattice-match conditions which lead to preferred orientations on four different Al_2O_3 surface planes. We further add to the library of VO_2 crystal-growth substrates by introducing YSZ, showing again the effects of chemical reactions and lattice match. Finally, comparing the growth habits of platelet-like and wire-like VO_2 crystals, our results suggest that strong lattice match disfavors the growth of crystals with low in-plane aspect ratios, while high surface energy favors the growth of large-area crystals, often with low aspect ratios. Choice of the substrate is a powerful but complex tool for designing VO_2 crystals, with surface energy, lattice matching, and chemical effects acting in concert to determine important properties of the resulting crystals.

EXPERIMENTAL SECTION

Single crystals of VO_2 were grown by the vapor-phase transport method. Vanadium pentoxide (V_2O_5) powder (Sigma-Aldrich, ≥99.6% trace metal basis) was loaded into one end of a quartz boat (100 mm × 17 mm × 10 mm, MTI) encrusted with a coat of vanadium oxide crystals from previous growths. Growth substrates were placed in the boat at varying distances from the precursor powder, tilted relative to the horizontal by leaning against the side of the boat (see Supporting Information, Section S3, Figure S2 for an image of the prepared boat before and after growth). Two filled boats were placed end-to-end inside a small quartz tube (235 mm × 26 mm dia.), which was then centered in a quartz tube furnace (Lindberg Blue M) at room temperature. The tube was evacuated with a vacuum pump and Ar gas was flowed at 25 sccm to achieve a stable pressure of 1.7 Torr. The flow direction was from the precursor toward substrates. The furnace was heated to 810 °C, held at that temperature for 1−4 h, and allowed to cool back to room

https://doi.org/10.1021/acs.cgd.1c00088
Cryst. Growth Des. 2021, 21, 3770−3778

temperature. As the temperature ramps up, the precursor melts and the gas flow carries resulting vanadia vapor to the substrates. Holding the system at a high temperature allows VO_2 to grow through a droplet-assisted growth mechanism. Droplets of the melted precursor condense onto the substrate, out of which VO_2 wires crystallize.[16,19,26]

Substrates, listed in Table 1, were purchased from MTI as wafers or precut chips, all polished on both sides. Wafers were cut into chips using a dicing saw or manually cleaved with a diamond scribe. Substrates were used as-received from the supplier without additional cleaning, as we found that cleaning had no significant effect on growth results.

Polarized optical microscopy was used to image the crystals and the ferroelastic twins. A Raman microscope (Thermo Scientific DXR, 532 nm) was used to distinguish the phases of VO_2 and to identify other species formed during growth. An X-ray diffractometer (Rigaku Smart Lab, Cu Kα source) was used to perform standard θ–2θ measurements (scan 2θ from 20 to 100°, 0.01° steps, 10°/min) and pole figure measurements (fix 2θ, scan α 0–90° in 1 or 3° steps, scan β 0–360° in 1 or 3° steps at 60 or 150°/min) to identify out-of-plane and in-plane crystal orientations, respectively. Energy-dispersive spectroscopy (EDS) measurements were carried out with a scanning electron microscope (Zeiss Merlin with Gemini II column) at 20 kV, 3 nA, and a working distance of 8.5 mm. Elemental analysis was performed with proprietary Oxford Instruments AZtec software.

RESULTS AND DISCUSSION

The following experimental results are divided into three subsections—considering first, the chemical and lattice-match effects of sapphire substrates, then those of yttria-stabilized zirconia (YSZ), and finally, comparing the crystal sizes and growth habits across different substrates. Raman spectroscopy shows that VO_2 crystals grown on sapphire are in the M2 phase, and EDS (Figure 1) shows the presence of Al dopants. Pole figure measurements (Figure 2) allow determination of crystal orientation and lattice-matching with the substrate (Table 2), including an orientation on *c*-cut (Figure 3) that is different (with better lattice match) than has been previously reported. Likewise, Raman spectra indicate the presence of ZrO_2 and YVO_4 on YSZ substrates after growth, and pole figures show a preferred orientation (Figure 4). Comparison of crystal size across substrates (Figure 5) shows that maximum crystal size tends to increase with substrate surface energy.

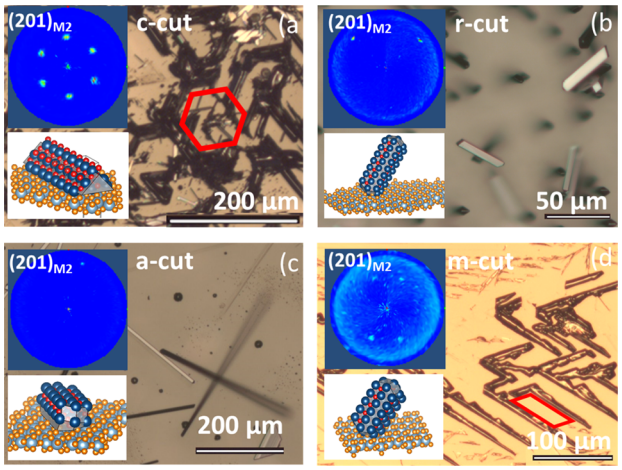

Figure 2. Microscope images of VO_2 crystals on the four sapphire cuts illustrate the preferred orientation of crystal growth. Insets (upper): X-ray diffractometry (XRD) pole figures show a preferred orientation on all four samples. Insets (lower): diagrams illustrating a crystal lattice orientation of epitaxial crystals, shown with the typical $(001)_R$ growth axis and $(110)_R$ side facets.

Growth on Sapphire. We examine VO_2 crystal growth on the following different cuts of sapphire (Al_2O_3): *c*- (0001), *r*- ($1\bar{1}02$), *a*- ($11\bar{2}0$), and *m*-cut ($1\bar{1}00$). Among typical VO_2 substrates, sapphire provides a good lattice match—domain-matching epitaxy of thin films on *c*-cut sapphire is well-established,[30] and epitaxial single crystals have been observed on *c*-, *r*-, *a*-, and *m*-cuts. Titanium dioxide (TiO_2) would offer a still better lattice match, but lower cost has rendered Al_2O_3 a common growth substrate, making its often-overlooked Al-doping (see discussion below) a relevant issue. This, and a better-characterized surface energy, makes sapphire of interest for this study.

On all the sapphire substrates, the vast majority of VO_2 crystals (30 out of 34 sampled) are in a secondary monoclinic phase (M2) at room temperature rather than the typical M1. Figure 1a compares Raman spectra from a representative VO_2 crystal grown on sapphire above (M2 phase, yellow curve) and below (T phase, red curve) room temperature to that of a crystal grown on quartz at room temperature (M1 phase, blue curve). It is well-known that tensile strain along the c_R axis[31] or compressive strain normal to it[32] can stabilize the M2 phase, and some reports observing M2-phase crystals on sapphire substrates have attributed this to substrate-induced strain.[33,34] However, the M2 phase can also be stabilized by Al-doping,[29] and molten vanadia is known to be corrosive to refractory oxides, including Al_2O_3.[35−37] Moreover, Nag et al. found that VO_2 films made with pulsed laser deposition at high temperatures (~500 °C) show a thin interlayer of non-stoichiometric Al, V, and O,[38] and Strelcov et al. have intentionally doped VO_2 crystals with Al by growing them on a thin film of Al_2O_3.[29] To determine which of the two mechanisms (strain or doping) is primarily responsible, we analyzed Raman spectra from a VO_2 crystal after removing it from the substrate with flexible adhesive tape. Thus freed from substrate strain, the crystal remained in the M2 phase, supporting the idea that doping is responsible for stabilizing this phase in our samples. As further confirmation, EDS measurements (Figure 1b) demonstrate the presence of Al in another VO_2 crystal removed from its substrate in the same manner.

We conclude that during the growth process, a small amount of the Al_2O_3 substrate is dissolved into molten vanadia droplets, and a small fraction of Al atoms is incorporated into the VO_2 lattice as it crystallizes from the droplet. We also note that etch pits appeared in many of the sapphire substrates after growth, which we attribute to the corrosive action of molten vanadia on the substrate (Supporting Information, Section S4, Figure S3).

While the orientation of the substrate does not seem to affect the doping and room-temperature phase of the crystals, it has a drastic impact on the morphology and orientation of the crystals. Figure 2 shows optical microscope images of some VO_2 crystals grown on sapphire substrates. Across multiple growth attempts on identical substrates, and even across a given sample, a variety of crystal sizes, shapes, and orientations can be observed; however, on all substrates, these crystals can broadly be grouped into two categories: crystals exhibiting a preferred orientation relative to each other and the substrate and crystals with a seemingly random orientation. The former (exemplified in Figure 2) tends to be fairly uniform on a given substrate, to be long and narrow in shape and to have facets

https://doi.org/10.1021/acs.cgd.1c00088
Cryst. Growth Des. 2021, 21, 3770−3778

Table 2. Observed Orientation and Calculated Lattice Match for VO_2 Crystals Grown on Various Cuts of Sapphire

Al_2O_3 cut	crystal orientation	lattice mismatch $\left(\frac{d_R - d_{Al_2O_3}}{d_{Al_2O_3}}\right)$	d_R (Å)	$d_{Al_2O_3}$ (Å)
c-cut $\{0001\}$	<keep-together>$\{100\}_R \| \{0001\}_{Al_2O_3}$ $\{011\}_R \| \{11\bar{2}0\}_{Al_2O_3}$</keep-together>	normal to matched plane: 0.6%	$\{011\}_R$:(2.42) × 1	<keep-together>$\{11\bar{2}0\}_{Al_2O_3}$:(2.40) × 1</keep-together>
		along matched plane: −3.2%	$\langle 01\bar{1}\rangle_R$:(5.37) × 3	<keep-together>$\langle 10\bar{1}0\rangle_{Al_2O_3}$:(8.32) × 2</keep-together>
r-cut $\{1\bar{1}02\}$	<keep-together>$\{011\}_R \| \{1\bar{1}02\}_{Al_2O_3}$ $\langle 100\rangle_R \| \langle 1\bar{2}10\rangle_{Al_2O_3}$</keep-together>	along matched vector: −5.2%	$\langle 100\rangle_R$:(4.55) × 1	<keep-together>$\langle 1\bar{2}10\rangle_{Al_2O_3}$:(4.81) × 1</keep-together>
		normal to matched vector: 3.7%	$\langle 01\bar{1}\rangle_R$:(5.37) × 3	<keep-together>$\langle \bar{1}01\bar{1}\rangle_{Al_2O_3}$:(15.53) × 1</keep-together>
a-cut $\{11\bar{2}0\}$	<keep-together>$\{210\}_R \| \{11\bar{2}0\}_{Al_2O_3}$ $\langle 1\bar{2}3_R\rangle \| \langle 0001\rangle_{Al_2O_3}$</keep-together>	along matched vector: 1.4%	$\langle 1\bar{2}3\rangle_R$:(13.30) × 1	<keep-together>$\langle 0001\rangle_{Al_2O_3}$:(13.12) × 1</keep-together>
		normal to matched vector: −1.6%	$\{30\bar{1}\}_R^a$:(2.18) × 5	$\{2\bar{1}\bar{1}0\}^a_{Al_2O_3}$: (2.77) × 4
m-cut $\{10\bar{1}0\}$	<keep-together>$\{031\}_R \| \{10\bar{1}0\}_{Al_2O_3}$ $\langle 100\rangle_R \| \langle 0001\rangle_{Al_2O_3}$</keep-together>	along matched vector: 4.2%	$\langle 100\rangle_R$:(4.55) × 3	<keep-together>$\langle 0001\rangle_{Al_2O_3}$:(13.12) × 1</keep-together>
		normal to matched vector: 0.8%	$\langle 0\bar{1}3\rangle_R$:(9.69) × 1	<keep-together>$\langle 1\bar{2}10\rangle_{Al_2O_3}$:(4.81) × 2</keep-together>

[a]These planes are not normal to the substrate surface, so the lattice match condition relates to the period of their intersections with the substrate plane, equal to $d/\sin(\theta)$ where θ is the angle between the plane and the surface.

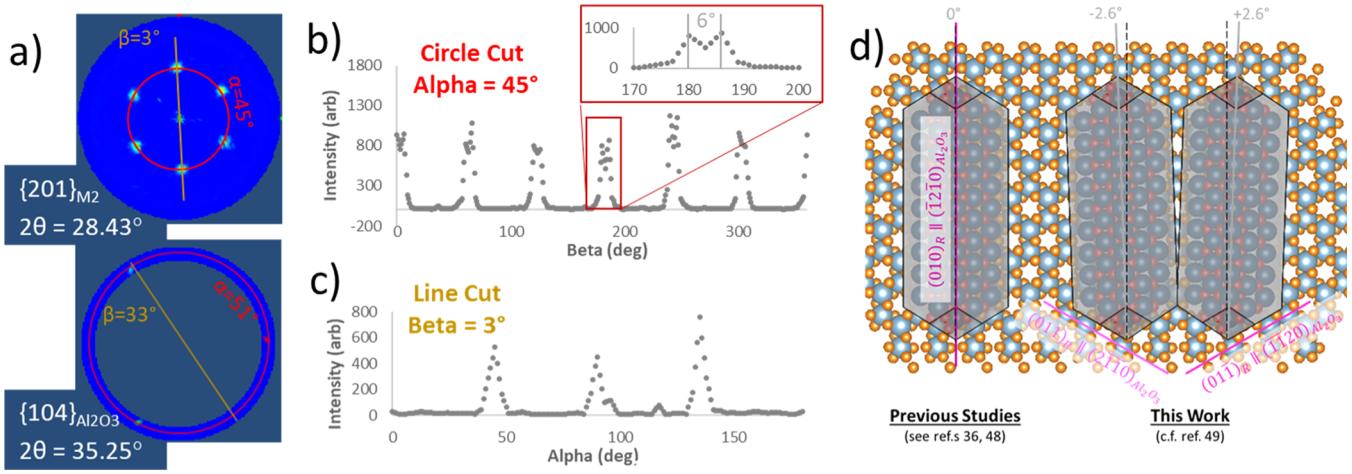

Figure 3. Orientation analysis for VO_2 crystals grown on *c*-cut sapphire. (a) Pole figures for the $\{201\}_{M2}$ and $\{104\}Al_2O_3$ sets of planes show their respective orientations and symmetries. Taking a circle cut (constant-α, panel b) or a line cut (constant-β, panel c) shows the in-plane orientation or out-of-plane tilt, respectively. A closer look at the $\{201\}_{M2}$ data (panel b, inset) reveals that each peak is split by ∼6° in β. These data allow quantitative determination of the relative orientations of the VO_2 and Al_2O_3 lattices (d).

nonparallel to the substrate surface, with cross-sectional shape determined by lattice orientation and energetically favored bounding facets. The latter (see Supporting Information, Section S5, Figure S4) is more varied in shape, size, and orientation but tends to have lower aspect ratios and to lie flat with their largest facets parallel to the substrate surface.

Powder XRD pole figure measurements provide a quantitative measurement of the orientations of a given crystalline plane in a sample; in our case, not for an individual single crystal but of all the crystals on a sample in aggregate. The upper insets in Figure 2 show pole figures for the $(201)_{M2}$ plane—equivalent to the $(110)_R$ or $(01\bar{1})_{M1}$ planes in other phases—which is usually the favored plane for side facets of VO_2 crystals.[27] Comparing the four pole figures in Figure 2, it is noticeable that they all have in common a peak at the center of the figure, corresponding to the normal to the substrate. This indicates that all of the samples have some VO_2 crystals with their $(201)_{M2}$ planes parallel to the substrate surface. These can be identified with the less-uniform, flat-lying, lower-aspect-ratio crystals present in all the samples, as noted above. Apart from this common central peak, each substrate presents a unique pattern corresponding to the preferred orientations of VO_2 crystals on that substrate. On *c*-cut sapphire (Figure 2a), a sixfold symmetry is evident, arising from the sixfold symmetry of the *c*-plane in the hexagonal sapphire lattice. On *m*-cut, likewise, a clear twofold symmetry emerges from the twofold symmetry of the substrate. Interestingly, the twofold symmetries of the *a*- and *r*-planes are not reflected in the corresponding VO_2 pole figures—it may be that asymmetry in the growth conditions (tilted sample and unidirectional vapor flow) caused one orientation to be preferred or that random fluctuations and sparse coverage resulted in one orientation

https://doi.org/10.1021/acs.cgd.1c00088
Cryst. Growth Des. 2021, 21, 3770−3778

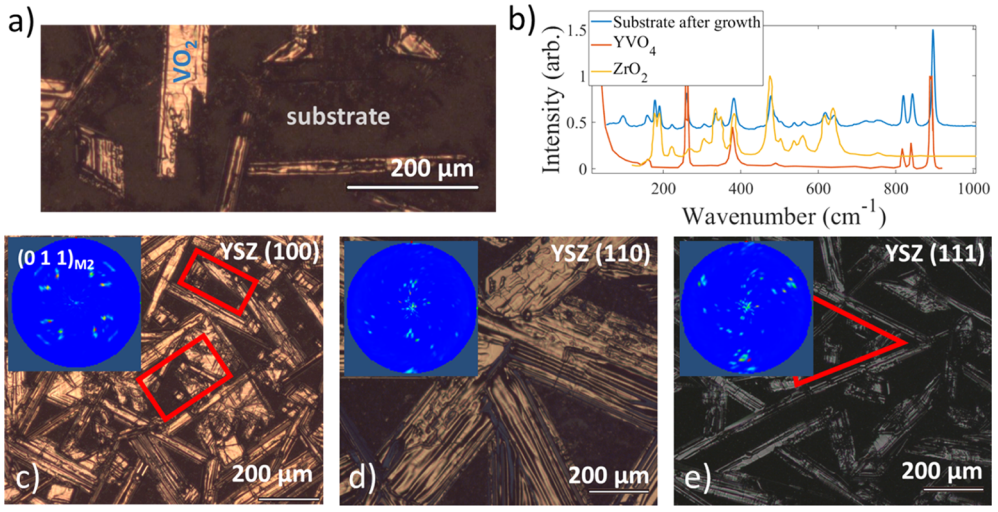

Figure 4. (a) Microscope image of VO_2 crystals grown on YSZ, and a dark film covering the substrate. (b) Raman spectra of the background film after growth (blue) show it to be composed of YVO_4 (red) and ZrO_2 (yellow). (c–e) Microscope images of VO_2 crystals grown on the three YSZ cuts investigated suggest a preferred orientation, confirmed by XRD pole figures (insets).

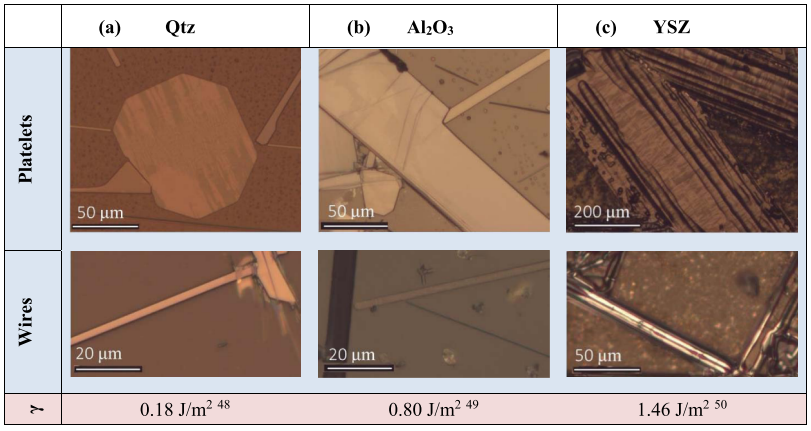

Figure 5. Examples of platelet- and wire-shaped VO_2 microcrystals. The platelets shown are representative of the largest we have produced. On every substrate, both morphologies are observed, with a range of sizes; however, the largest crystals on sapphire tend to be slightly larger than those on quartz, while the crystals on YSZ far exceed either of the others in size. This size ordering follows the surface energies (γ) of the substrates (extrapolated to 810 °C). Note the different scale bars in each image.

occurring so infrequently as to be lost in noise. The different orientations determined for each substrate (see discussion below) are illustrated in the lower insets in Figure 2, assuming the energetically favorable $(001)_R$ growth axis and $(110)_R$ side facets.

By comparing these pole figures for VO_2 crystal planes to similar ones for the substrate planes, it is possible to determine the preferred orientation(s) of the VO_2 crystals relative to the substrate lattice. Figure 3 details such an analysis for crystals grown on *c*-cut sapphire (the corresponding analysis for other substrates is found in the Supporting Information, Section S6, Figures S5–S7, and Table S3). For simplicity, from this point forward, we reference the VO_2 crystal planes according to the equivalent planes of the R phase, since this is the phase of the crystals during growth and thus the phase relevant for lattice-match considerations affecting the growth. The pole figure (Figure 3a) for $\{110\}_R$ has a peak at $\alpha = 90°$ ($\{110\}_R$ parallel to substrate) and six at $\alpha = 45°$ ($\{100\}_R$ parallel to substrate) and $\beta = 3° + n(60°)$ ($n = 0,1,2,3,4,5$), the sixfold symmetry reflecting the hexagonal lattice of the $\{0001\}_{Al_2O_3}$ plane. A pole figure for $\{10\bar{1}4\}_{Al_2O_3}$ on the same sample has three peaks at $\alpha = 52°$ and $\beta = 33° + n(120°)$ ($n = 0,1,2$), as expected for these planes relative to $\{0001\}_{Al_2O_3}$. Comparing these, the $\{110\}_R$ planes appear with $\Delta\beta = \pm 90°$ relative to $\{10\bar{1}4\}_{Al_2O_3}$, consistent with the orientation $\{010\}_R \| \{11\bar{2}0\}_{Al_2O_3}$ (Figure 3d, left), which is equivalent to that reported in previous studies on single crystals[25] and thin films.[39] However, looking more closely at the $\{110\}_R$ pole figure (Figure 3b), it appears that each peak is split into two, with a separation of ~6° in β. This can be explained if instead $\{011\}_R \| \{11\bar{2}0\}_{Al_2O_3}$ (Figure 3d, right), the 6° splitting arising because of $\{011\}_R$ are separated from $\{010\}_R$ by ±57° as noted in one study on thin films.[40] Moreover, we find that this orientation yields better lattice match (see Table S2): 0.6% (−3.2%) mismatch normal (parallel) to the matched plane, as opposed to 3.7% (−5.2%) for the conventional orientation. The results of orientation analysis on other cuts of Al_2O_3, including lattice mismatch calculations, are summarized in Table 2. Except on *a*-cut (see discussion accompanying Supporting Information, Figure S7), the crystallographic orientation is derived from multiple peaks in the XRD pole figures for both $\{201\}_{M2}$ and $\{220/021\}_{M2}$

https://doi.org/10.1021/acs.cgd.1c00088
Cryst. Growth Des. 2021, 21, 3770–3778

sets of planes, guaranteeing a unique orientation. Lattice mismatch is calculated by finding the percent difference between matched plane spacings (or lattice vector lengths) d, with VO_2 crystallographic parameters drawn from the literature.[41]

Growth on YSZ. YSZ is a form of zirconia (ZrO_2) stabilized in its cubic phase by doping with yttria (Y_2O_3). Ceramic YSZ is of interest as a refractory material for solid-oxide fuel cells, high-temperature turbine coatings, and nuclear reactor fuel matrices,[42] and erbium-doped single-crystal YSZ has been used for upconversion luminescence.[43] YSZ thin films have been used as a buffer layer to grow epitaxial VO_2 films on Si substrates,[44] suggesting that the YSZ and VO_2 lattices may be close enough to result in a preferred orientation.

After growth on YSZ, the entire substrate (initially transparent) is covered with a dark film, as well as assorted VO_2 crystals (Figure 4a). Analysis of this dark film with Raman spectroscopy (Figure 4b, blue curve) clearly shows peaks belonging to yttrium vanadate (YVO_4, red curve) and zirconia (ZrO_2, yellow curve). At high temperatures, YSZ is known to become unstable, tending to form yttria-rich and yttria-poor domains;[45] moreover, near 800 °C, vanadia is known to react with yttria in YSZ to form yttrium vanadate,[46,47] as we observe. By removing VO_2 crystals from the substrate with adhesive tape, it is observed that the layer of YVO_4/ZrO_2 underlies the VO_2 crystals (Supporting Information, Section S7, Figure S8). From this and the uniformity of the YVO_4/ZrO_2 layer, we hypothesize that, rather than forming individual droplets, molten vanadia completely wets the YSZ surface during growth and reacts with the substrate; VO_2 crystals then grow atop the resulting YVO_4 layer. The VO_2 crystals grown thus tend to be large (tens to hundreds of micrometers in width), which we attribute to the aforementioned surface wetting, and to have rough surfaces, as seen in the optical micrographs (Figure 4a,c−e). All the crystals sampled are in the usual M1 phase at room temperature.

On each of the three cuts of YSZ, there is clear evidence of the preferred orientation. While none of these grow out-of-plane (as on some cuts of sapphire), the in-plane growth axis $(001)_R$ tends to orient along certain directions, causing groups of crystals to form rectangular or triangular patterns (Figure 4c−e). Pole figures confirm this qualitative observation, showing distinct and complex patterns with fourfold, twofold, and threefold symmetry reflecting the respective symmetries of the (100), (110), and (111) planes of cubic YSZ. Determining a definite lattice-match relation to the substrate, however, is complicated by the fact that a layer or layers of YVO_4 and ZrO_2 lie between the VO_2 crystals and the substrate. Pole figure measurements for distinctive planes of these materials (Supporting Information, Section S8, Figure S9) show that they, too, have definite preferred orientations relative to the underlying YSZ. This suggests that the situation is one multilayer heteroepitaxy, where the lower-symmetry YVO_4 and ZrO_2 may have multiple distinguishable orientations relative to the higher-symmetry substrate, leading to the complex peak-splitting patterns observed for VO_2. A full analysis of the orientation and lattice mismatch of each layer is beyond the scope of this paper.

Substrate Effects on Nanowire/Microplatelet Size. The size and aspect ratio of VO_2 crystals are affected by growth conditions (time, temperature, pressure, and precursor) but are difficult to precisely control. Generally, increasing the flux of precursor vapor (by increasing the amount of precursor or placing samples closer to the precursor source) will result in larger crystals with a lower aspect ratio and vice versa. Although we have attempted to optimize for the growth of larger crystals, the resulting crystal sizes vary drastically due to variables such as sample orientation, residual precursor, or stochastic precursor droplet aggregation. Our results emphasize that the substrate also strongly affects whether high-aspect-ratio nanowires or low-aspect-ratio microplatelets are preferred (Figure 5). On quartz (Figure 5a), both forms are observed, often coexisting on the same sample (see Supporting Information, Section S9, Figure S10 for a discussion of the crystal growth results on quartz). Which predominates is somewhat random but strongly affected by the growth parameters. The largest crystals are often in excess of 50 by 50 μm. On sapphire (Figure 5b), nanowires and microplatelets (in some cases even larger than any seen on quartz) are again observed to coexist; however, as noted above, the nanowires tend to exhibit a preferred orientation and to have facets nonparallel to the substrate (with some exceptions, nanowires with parallel and nonparallel facets can both be seen in Figure 5b), while the microplatelets (like those on quartz) seem to have no preferred orientation in-plane and always have facets parallel to the substrate. The former is attested in the literature, with most studies of epitaxial VO_2 crystals on sapphire exhibiting nanowire growth; the latter has not been reported. This suggests that epitaxy on sapphire disfavors low-aspect-ratio growth presumably because the increased contact area increases the total amount of lattice mismatch strain, whereas those crystals which form without epitaxy are free from this constraint, much like those that grow on a substrate with no lattice matching. Crystals grown on YSZ, on the other hand (Figure 5c), tend to be larger with a low aspect ratio. Most of these crystals are larger than on any other substrate we investigated, and a few are larger than any yet reported to be grown by vapor transport methods, in excess of 1 mm in length.

In addition to chemical reactions and lattice matching effects, a third interaction is likely to play a strong role in determining the crystal morphologies that are possible on a given substrate: surface/interface energies and the wettability of the substrate by molten V_2O_5. This will affect the size and shape of precursor droplets and thus also the resulting crystals. Figure 5 presents representative surface energies (where available) for the different substrates used in this study.[48−50] It is noteworthy that the surface energy increases in the order $\gamma_{qtz} < \gamma_{Al2O3} < \gamma_{YSZ}$, the same order followed by the maximum microcrystal size. This suggests that substrate surface energy is a key factor in determining the size of VO_2 crystals grown by this method: greater surface energy leads to better wetting by the V_2O_5 precursor, which in turn results in larger V_2O_5 droplets, more substrate coverage, and, ultimately, larger crystals. We consider this a topic well worth further investigation, hypothesizing that for the growth of large-area microplatelets, high surface energy is more important than good lattice match.

Summary of Experimental Results. Lattice-matching effects result in a preferred orientation on all cuts of sapphire and YSZ, although nonoriented crystals also appear in most cases. On sapphire, at least, it appears that oriented crystals are more likely than their nonoriented counterparts to have high aspect ratios, which we attribute to the effects of lattice-induced strain. On YSZ, the preferred orientation arises from multilayer heteroepitaxy, with highly oriented ZrO_2/YVO_4

https://doi.org/10.1021/acs.cgd.1c00088
Cryst. Growth Des. 2021, 21, 3770−3778

lying between VO_2 and the substrate. Chemical effects also play a prominent role, although they have received less attention heretofore. Molten vanadia can be highly reactive, even with refractory oxides such as Al_2O_3 and YSZ. On Al_2O_3 substrates, this results in etching of the substrate and Al-doping of the VO_2 crystals; this doping, rather than substrate-induced strain, is primarily responsible for these crystals relaxing to the M2, instead of the M1, phase when cooled to room temperature. On YSZ substrates, YVO_4 is formed at the substrate surface, forming a lattice-matched buffer layer between the substrate and VO_2 and representing (to the best of our knowledge) a novel method for the growth of YVO_4 films. We have also identified a third possible mechanism of substrate influence—its wettability by molten vanadia. Substrates with higher surface energies tend to grow larger crystals because the precursor vapor can more fully wet the substrate surface. This may also have an impact on the crystal morphology and is a ripe area for further study.

CONCLUSIONS

After over 60 years of research, a great deal of progress has been made in the fabrication of high-quality VO_2, but as its phase-transition behaviors are so exquisitely sensitive to its crystallite size, grain boundaries, dopants, strain states, and lattice defects, the ability to finely control its morphology is critical. Single crystals of VO_2, while offering a better platform to study its bulk properties and enabling device architectures difficult or impossible to achieve with thin films, are still hard to produce controllably and to reproduce consistently. Some progress has been made in the growth of highly uniform, oriented nanowires; however, large, low-aspect-ratio crystals suitable for optical experiments or 2D-material platforms are harder to obtain.

Among the dizzying array of growth parameters that can be tuned to influence crystal growth, choice of the substrate is a simple but powerful tool to engineer crystal morphology, as has been shown with lattice-match-oriented nanowires. Based on our results and a survey of other studies, we suggest a threefold paradigm for evaluating substrates to be used in VO_2 crystal growth (illustrated in Figure 6)—lattice match, which affects orientation, shape, and aspect ratio; chemical reactions with molten V_2O_5, which can result in doping of VO_2, changes to the substrate surface, or generation of interfacial species; and surface energy, which affects wetting of the surface by the V_2O_5 precursor and thus the size of and substrate coverage by VO_2 crystals.

Applying this paradigm can help to predict the results of VO_2 crystal growth, identify otherwise hard-to-find effects (such as small doping concentrations), and, ultimately, identify substrates likely to yield desired crystal properties. For example, TiO_2 is generally considered the ideal substrate for epitaxial VO_2 growth, due to its rutile crystal structure and excellent lattice match with VO_2 (see Supporting Information, Section S10, Table S4). We would expect that to result in highly oriented, high-aspect-ratio crystals, as have indeed been observed.[26,27] Additionally, there is potential for a slight amount of Ti-doping; although studies on TiO_2 surface energy are few, there is evidence that V_2O_5 wets the surface well (see discussion in the Supporting Information, Section S10). However, for yet another example, we predict that the growth of large, low-aspect-ratio crystals would be favored by substrates with high surface energy, low reactivity with VO_2, and little or no lattice match to VO_2. We anticipate that these considerations will help to guide further advancements in VO_2 crystal growth and engineering.

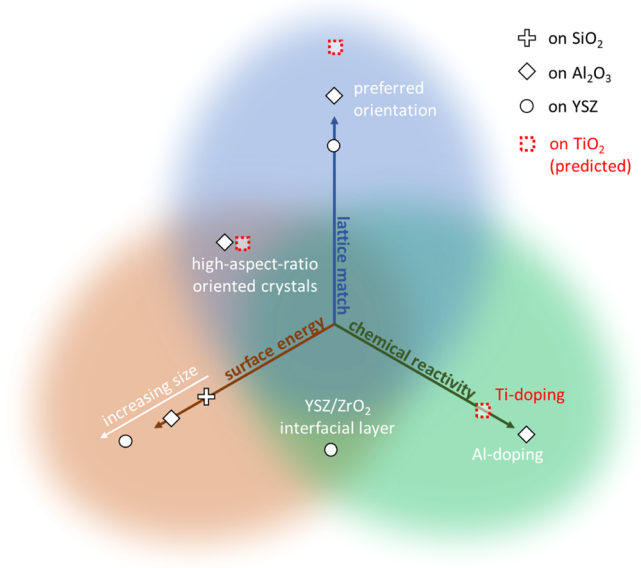

Figure 6. Schematic diagram depicting the different substrate properties that affect VO_2 crystal growth. Effects observed in this study are marked in white, those predicted for TiO_2 (an example case) in red.

ASSOCIATED CONTENT

Supporting Information

The Supporting Information is available free of charge at https://pubs.acs.org/doi/10.1021/acs.cgd.1c00088.

VO_2 crystal lattice and phases; review of progress in vapor transport growth; sample and precursor loading; etch pits in sapphire; examples of large, flat, low-aspect-ratio microcrystals on sapphire; analysis of pole figures on other cuts of sapphire; evidence that a YVO_4 layer underlies VO_2 crystals on YSZ; pole figures for YVO_4 and ZrO_2, on YSZ; growth results on quartz; and titanium dioxide substrate properties (PDF)

AUTHOR INFORMATION

Corresponding Authors

Samuel T. White − *Physics and Astronomy Department, Vanderbilt University, Nashville, Tennessee 37212, United States;* orcid.org/0000-0002-3168-8894; Email: samuel.t.white@vanderbilt.edu

Richard F. Haglund − *Physics and Astronomy Department, Vanderbilt University, Nashville, Tennessee 37212, United States;* orcid.org/0000-0002-2701-1768; Email: richard.haglund@vanderbilt.edu

Authors

Ellis A. Thompson − *Department of Physics, University of Washington, Seattle, Washington 98195, United States*

Peyton F. Brown − *Physics and Astronomy Department, Vanderbilt University, Nashville, Tennessee 37212, United States*

Complete contact information is available at: https://pubs.acs.org/10.1021/acs.cgd.1c00088

https://doi.org/10.1021/acs.cgd.1c00088
Cryst. Growth Des. 2021, 21, 3770−3778

Notes

The authors declare no competing financial interest.

■ ACKNOWLEDGMENTS

Optical microscopy, Raman microscopy, and SEM−EDS measurements were conducted at the Vanderbilt Institute of Nanoscale Science and Engineering. X-ray diffraction measurements were conducted at the Vanderbilt Chemistry Department Powder XRD Core with support from Evan Robinson and Christopher Sharp. E.A.T. acknowledges support from the National Science Foundation through grant number DMR-1560414. The material is based upon work supported by the National Aeronautics and Space Administration under Contract Number 80NSSC19C0207.

■ REFERENCES

(1) Ke, Y.; Wang, S.; Liu, G.; Li, M.; White, T. J.; Long, Y. Vanadium dioxide: The multistimuli responsive material and its applications. *Small* **2018**, *14*, 1802025.
(2) Liu, K.; Lee, S.; Yang, S.; Delaire, O.; Wu, J. Recent progresses on physics and applications of vanadium dioxide. *Mater. Today* **2018**, *21*, 875−896.
(3) Shao, Z.; Cao, X.; Luo, H. J.; Jin, P. Recent progress in the phase-transition mechanism and modulation of vanadium dioxide materials. *NPG Asia Mater.* **2018**, *10*, 581−605.
(4) Shi, R.; Shen, N.; Wang, J.; Wang, W.; Amini, A.; Wang, N.; Cheng, C. Recent advances in fabrication strategies, phase transition modulation, and advanced applications of vanadium dioxide. *Appl. Phys. Rev.* **2019**, *6*, 011312.
(5) Liu, M.; Sternbach, A. J.; Basov, D. N. Nanoscale electrodynamics of strongly correlated quantum materials. *Rep. Prog. Phys.* **2017**, *80*, 014501.
(6) Yang, Z.; Ko, C. Y.; Ramanathan, S. Oxide Electronics Utilizing Ultrafast Metal-Insulator Transitions. In *Annual Review of Materials Research*; Clarke, D. R., Fratzl, P., Eds.; Annual Review, 2011; Vol. *41*, pp 337−367.
(7) Wegkamp, D.; Stähler, J. Ultrafast dynamics during the photoinduced phase transition in VO_2. *Prog. Surf. Sci.* **2015**, *90*, 464−502.
(8) Nag, J.; Haglund Jr, R. F. Synthesis of vanadium dioxide thin films and nanoparticles. *J. Phys.: Condens. Matter* **2008**, *20*, 264016.
(9) Vu, T. D.; Chen, Z.; Zeng, X.; Jiang, M.; Liu, S.; Gao, Y.; Long, Y. Physical vapour deposition of vanadium dioxide for thermochromic smart window applications. *J. Mater. Chem. C* **2019**, *7*, 2121−2145.
(10) Hallman, K. A.; Miller, K. J.; Baydin, A.; Weiss, S. M.; Haglund, R. F. Sub-Picosecond Response Time of a Hybrid VO2:Silicon Waveguide at 1550 nm. *Adv. Opt. Mater.* **2021**, *9*, 2001721.
(11) Tselev, A.; Strelcov, E.; Luk'yanchuk, I. A.; Budai, J. D.; Tischler, J. Z.; Ivanov, I. N.; Jones, K.; Proksch, R.; Kalinin, S. V.; Kolmakov, A. Interplay between ferroelastic and metal-insulator phase transitions in strained quasi-two-dimensional VO_2 nanoplatelets. *Nano Lett.* **2010**, *10*, 2003−2011.
(12) McGahan, C.; Gamage, S.; Liang, J.; Cross, B.; Marvel, R. E.; Haglund, R. F.; Abate, Y. Geometric constraints on phase coexistence in vanadium dioxide single crystals. *Nanotechnology* **2017**, *28*, 085701.
(13) Folland, T. G.; Fali, A.; White, S. T.; Matson, J. R.; Liu, S.; Aghamiri, N. A.; Edgar, J. H.; Haglund, R. F.; Abate, Y.; Caldwell, J. D. Reconfigurable infrared hyperbolic metasurfaces using phase change materials. *Nat. Commun.* **2018**, *9*, 4371.
(14) Cheng, C.; Guo, H.; Amini, A.; Liu, K.; Fu, D.; Zou, J.; Song, H. S. Self-assembly and horizontal orientation growth of VO_2 nanowires. *Sci. Rep.* **2014**, *4*, 5456.
(15) Cheng, C.; Liu, K.; Xiang, B.; Suh, J.; Wu, J. Ultra-long, free-standing, single-crystalline vanadium dioxide micro/nanowires grown by simple thermal evaporation. *Appl. Phys. Lett.* **2012**, *100*, 103111.
(16) Cheng, Y.; Wong, T. L.; Ho, K. M.; Wang, N. The structure and growth mechanism of VO_2 nanowires. *J. Cryst. Growth* **2009**, *311*, 1571−1575.
(17) Guiton, B. S.; Gu, Q.; Prieto, A. L.; Gudiksen, M. S.; Park, H. Single-crystalline vanadium dioxide nanowires with rectangular cross sections. *J. Am. Chem. Soc.* **2005**, *127*, 498−499.
(18) Kim, I. S.; Lauhon, L. J. Increased yield and uniformity of vanadium dioxide nanobeam growth via two-step physical vapor transport process. *Cryst. Growth Des.* **2012**, *12*, 1383−1387.
(19) Kim, M.-W.; Ha, S.-S.; Seo, O.; Noh, D. Y.; Kim, B.-J. Real-time structural and electrical characterization of metal-insulator transition in strain-modulated single-phase VO_2 wires with controlled diameters. *Nano Lett.* **2016**, *16*, 4074−4081.
(20) Lin, J.; Ji, H.; Swift, M. W.; Hardy, W. J.; Peng, Z.; Fan, X.; Nevidomskyy, A. H.; Tour, J. M.; Natelson, D. Hydrogen diffusion and stabilization in single-crystal VO_2 micro/nanobeams by direct atomic hydrogenation. *Nano Lett.* **2014**, *14*, 5445−5451.
(21) Löffler, S.; Auer, E.; Weil, M.; Lugstein, A.; Bertagnolli, E. Impact of growth temperature on the crystal habits, forms and structures of VO_2 nanocrystals. *Appl. Phys. A: Mater. Sci. Process.* **2011**, *102*, 201−204.
(22) Maeng, J.; Kim, T.-W.; Jo, G.; Lee, T. Fabrication, structural and electrical characterization of VO_2 nanowires. *Mater. Res. Bull.* **2008**, *43*, 1649−1656.
(23) Sidorov, A. I.; Lyubimov, V. Y.; Nashchekin, A. V. Morphological features of vanadium dioxide microcrystals grown from the gas phase. *Tech. Phys. Lett.* **2007**, *33*, 955−957.
(24) Sohn, J. I.; Joo, H. J.; Ahn, D.; Lee, H. H.; Porter, A. E.; Kim, K.; Kang, D. J.; Welland, M. E. Surface-stress-induced mott transition and nature of associated spatial phase transition in single crystalline VO_2 nanowires. *Nano Lett.* **2009**, *9*, 3392−3397.
(25) Sohn, J. I.; Joo, H. J.; Porter, A. E.; Choi, C.-J.; Kim, K.; Kang, D. J.; Welland, M. E. Direct observation of the structural component of the metal-insulator phase transition and growth habits of epitaxially grown VO_2 nanowires. *Nano Lett.* **2007**, *7*, 1570−1574.
(26) Strelcov, E.; Davydov, A. V.; Lanke, U.; Watts, C.; Kolmakov, A. In situ monitoring of the growth, intermediate phase transformations and templating of single crystal VO_2 nanowires and nanoplatelets. *ACS Nano* **2011**, *5*, 3373−3384.
(27) Wang, L.; Ren, H.; Chen, S.; Chen, Y.; Li, B.; Zou, C.; Zhang, G.; Lu, Y. Epitaxial growth of well-aligned single-crystalline VO_2 micro/ nanowires assisted by substrate facet confinement. *Cryst. Growth Des.* **2018**, *18*, 3896−3901.
(28) Wu, J.; Gu, Q.; Guiton, B. S.; de Leon, N. P.; Ouyang, L.; Park, H. Strain-induced self organization of metal-insulator domains in single-crystalline VO_2 nanobeams. *Nano Lett.* **2006**, *6*, 2313−2317.
(29) Strelcov, E.; Tselev, A.; Ivanov, I.; Budai, J. D.; Zhang, J.; Tischler, J. Z.; Kravchenko, I.; Kalinin, S. V.; Kolmakov, A. Doping-based stabilization of the M2 phase in free-standing VO_2 nanostructures at room temperature. *Nano Lett.* **2012**, *12*, 6198−6205.
(30) Narayan, J.; Bhosle, V. M. Phase transition and critical issues in structure-property correlations of vanadium oxide. *J. Appl. Phys.* **2006**, *100*, 103524.
(31) Cao, J.; Gu, Y.; Fan, W.; Chen, L. Q.; Ogletree, D. F.; Chen, K.; Tamura, N.; Kunz, M.; Barrett, C.; Seidel, J.; Wu, J. Extended mapping and exploration of the vanadium dioxide stress-temperature phase diagram. *Nano Lett.* **2010**, *10*, 2667−2673.
(32) Pouget, J. P.; Launois, H.; D'Haenens, J. P.; Merenda, P.; Rice, T. M. Electron localization induced by uniaxial stress in pure VO_2. *Phys. Rev. Lett.* **1975**, *35*, 873−875.
(33) Jones, A. C.; Berweger, S.; Wei, J.; Cobden, D.; Raschke, M. B. Nano-optical investigations of the metal-insulator phase behavior of individual VO_2 microcrystals. *Nano Lett.* **2010**, *10*, 1574−1581.
(34) Sohn, J. I.; Joo, H. J.; Kim, K. S.; Yang, H. W.; Jang, A.-R.; Ahn, D.; Lee, H. H.; Cha, S.; Kang, D. J.; Kim, J. M.; Welland, M. E. Stress-induced domain dynamics and phase transitions in epitaxially grown VO_2 nanowires. *Nanotechnology* **2012**, *23*, 205707.

https://doi.org/10.1021/acs.cgd.1c00088
Cryst. Growth Des. 2021, 21, 3770−3778

(35) Katz, J. D.; Hurley, G. Etching alumina with molten vanadium pentoxide. *J. Am. Ceram. Soc.* **1990**, *73*, 2151−2152.
(36) Safdar, M.; Frischat, G. H.; Salge, H. Etching of Al_2O_3 surfaces with molten V_2O_5. *J. Am. Ceram. Soc.* **1974**, *57*, 106.
(37) Sequeira, C. A. C.; Chen, Y.; Marquis, F. D. S. Solubility of silica and alumina in sodium sulphate-sodium vanadate-vanadium pentoxide melts. In *High Temperature Corrosion in Molten Salts*; Sequeira, C. A. C., Ed.; Trans Tech Publications Ltd: Switzerland, 2003; Vol. 7, pp 335−348.
(38) Nag, J.; Payzant, E. A.; More, K. L.; Haglund, R. F. Enhanced performance of room-temperature-grown epitaxial thin films of vanadium dioxide. *Appl. Phys. Lett.* **2011**, *98*, 251916.
(39) Wong, F. J.; Zhou, Y.; Ramanathan, S. Epitaxial variants of VO_2 thin films on complex oxide single crystal substrates with 3m surface symmetry. *J. Cryst. Growth* **2013**, *364*, 74−80.
(40) Chen, C.; Zhu, Y.; Zhao, Y.; Lee, J. H.; Wang, H.; Bernussi, A.; Holtz, M.; Fan, Z. VO_2 multidomain heteroepitaxial growth and terahertz transmission modulation. *Appl. Phys. Lett.* **2010**, *97*, 211905.
(41) McWhan, D. B.; Marezio, M.; Remeika, J. P.; Dernier, P. D. X-ray-diffraction study of metallic VO_2. *Phys. Rev. B: Solid State* **1974**, *10*, 490−495.
(42) Cousland, G. Investigation of material properties of yttria-stabilised zirconia using experimental techniques and first-principles calculations, Ph.D Doctorate, University of Sydney, Sydney, Australia, 2014.
(43) Wang, X.; Tan, X.; Xu, S.; Liu, F.; Goodman, B. A.; Deng, W. Preparation and up-conversion luminescence of Er-doped yttria stabilized zirconia single crystals. *J. Lumin.* **2020**, *219*, 116896.
(44) Gupta, A.; Aggarwal, R.; Gupta, P.; Dutta, T.; Narayan, R. J.; Narayan, J. Semiconductor to metal transition characteristics of VO_2 thin films grown epitaxially on Si (001). *Appl. Phys. Lett.* **2009**, *95*, 111915.
(45) Butz, B.; Schneider, R.; Gerthsen, D.; Schowalter, M.; Rosenauer, A. Decomposition of 8.5 mol.% Y_2O_3-doped zirconia and its contribution to the degradation of ionic conductivity. *Acta Mater.* **2009**, *57*, 5480−5490.
(46) Hertl, W. Vanadia reactions with yttria stabilized zirconia. *J. Appl. Phys.* **1988**, *63*, 5514−5520.
(47) Susnitzky, D. W.; Hertl, W.; Carter, C. B. Vanadia-induced transformations in yttria-stabilized zirconia. *Ultramicroscopy* **1989**, *30*, 233−241.
(48) Janczuk, B.; Zdziennicka, A. A study on the components of surface free-energy of quartz from contact-angle measurements. *J. Mater. Sci.* **1994**, *29*, 3559−3564.
(49) Rhee, S. K. Critical surface energies of Al_2O_3 and graphite. *J. Am. Ceram. Soc.* **1972**, *55*, 300−303.
(50) Tsoga, A.; Nikolopoulos, P. Surface and grain-boundary energies in yttria-stabilized zirconia (YSZ-8 mol %). *J. Mater. Sci.* **1996**, *31*, 5409−5413.

https://doi.org/10.1021/acs.cgd.1c00088
Cryst. Growth Des. 2021, 21, 3770−3778